Original Article

AOSPINE

Global Spine Journal
2018, Vol. 8(5) 460-470

DOI: 10.1177/2192568217735802
journals.sagepub.com/home/gsj
SAGE

The Role of Sacral Slope in the Progression of a Bilateral Spondylolytic Defect at L5 to Spondylolisthesis: A Biomechanical Investigation Using Finite Element Analysis

Vivek A. S. Ramakrishna, BS[1,2], Uphar Chamoli, PhD[1], Luke L. Viglione, MBBS[1], Naomi Tsafnat, PhD[3], and Ashish D. Diwan, PhD, FRACS[1]

Abstract

Study Design: A biomechanical study using finite element analysis.

Objectives: The main objective of this study was to investigate the role of sacral slope in the progression of a L5 bilateral spondylolytic defect to spondylolisthesis.

Methods: A 3-dimensional model of lumbosacral spine was built using computed tomography (CT) data procured from an anonymized healthy male subject. The segmented CT data was manipulated to generate 3 more models representing L5 bilateral spondylolytic defect with normal sacral slope (SS), sacral slope increased by 10° (SS+10), and sacral slope decreased by 10° (SS-10). The 3D models were imported into finite element modelling software Strand7 for preprocessing, running nonlinear static solves, and postprocessing of the results.

Results: Directional biomechanical instabilities were induced in the lumbosacral spine as a result of changes in the L5-S1 disc shape secondary to the changes in sacral slope. Compared with the normal L5 lytic model, wedging of the L5-S1 disc (SS+10) resulted in a significantly greater range of motion in flexion (18% ↑) but extension motion characteristics were similar. Conversely, flattening of the L5-S1 disc (SS-10) resulted in a significantly greater range of motion in extension (16% ↑) but flexion motion characteristics were similar to that of the normal L5 lytic model.

Conclusions: Variations in sacral slope while preserving the L5-S1 mid-disc height and orientation of the L5 vertebra resulted in variations in the L5-S1 disc shape. The results suggest that for such extremities in the L5-S1 disc shape different pathomechanisms exist for the progression of the L5 lytic defect to spondylolisthesis.

Keywords

spondylolysis, spondylolisthesis, biomechanical instability, sacral slope, finite element analysis, L5-S1 disc shape, wedging

Introduction

Isthmic spondylolysis (or lytic defect) is characterized by a fracture to the pars interarticularis and occurs most commonly as a bilateral defect in the L5 vertebra.[1,2] The progression of the defect to spondylolisthesis occurs predominantly before the spine reaches skeletal maturity.[1] Previous studies have attempted to categorically define prognostic factors involved in the development and progression of the defect to spondylolisthesis, and clinical research conducted mostly through radiographic analysis has presented viable qualitative theories.[3-8]

[1] Spine Service, Department of Orthopaedic Surgery, St. George & Sutherland Clinical School, University of New South Wales Australia, Kogarah, Sydney NSW, Australia
[2] School of Biomedical Engineering, University of Technology Sydney, Ultimo NSW, Australia
[3] School of Mechanical and Manufacturing Engineering, University of New South Wales Australia, Kensington campus, Sydney NSW, Australia

Corresponding Author:
Uphar Chamoli, The Orthopaedic Research Institute, 4-10 South Street, Level 2—Research and Education Building, St. George Hospital Campus, Sydney, New South Wales 2217, Australia.
Email: u.chamoli@unsw.edu.au

In children and adolescents, progression to spondylolisthesis is attributed to growth plate injury that may perpetuate to epiphyseal ring separation.[8,9] In adults, the presence of a lytic defect could accelerate disc degeneration below the affected level, which may compromise a disc's ability to resist anterior shear forces and ultimately result in vertebral slippage.[10-12] Although rare in adults, progression to spondylolisthesis without any associated disc degeneration is reported in the literature.[13,14] It remains unclear whether disc degeneration is the cause or consequence of the vertebral slippage.

Spinopelvic morphology and orientation, measured using parameters such as pelvic incidence (PI), sacral slope (SS), pelvic tilt (PT), lumbar lordosis (LL), and C7 plumb line sagittal vertical axis (SVA), are thought to play an important role in maintaining sagittal balance of the lumbosacral spine; and any anomaly may result in a biomechanical environment leading to the development of the L5 lytic defect and its progression to spondylolisthesis.[3-6] Roussouly et al proposed "nutcracker" (low PI and low SS) and "shear-type" (high PI and high SS) mechanisms for the development of the defect in patients with abnormal spinopelvic parameters.[3] Oh et al observed that PI and SS were significantly higher in a spondylolysis (and low-grade spondylolisthesis) group of young males when compared with an age- and sex-matched control group of subjects without spondylolysis.[15] Vialle et al reported significantly higher PI and SS values in isthmic spondylolisthesis patients compared with controls.[7]

Patients with high-grade spondylolisthesis may have a balanced or unbalanced sagittal spinopelvic profile.[5] The position of the C7 plumb line SVA from the center of the femoral head is often used as a proxy to distinguish between a balanced (C7-SVA over or behind the bicoxo-femoral axis) and an unbalanced spine (in front of the bicoxo-femoral axis).[4] Labelle et al posited that an unbalanced spine has 2 compensatory mechanisms available to it to achieve a balanced posture, and when the maximal limits of the 2 mechanisms are reached, the patient develops a net sagittal trunk imbalance, mostly characterized either by compensatory hip flexion or forward leaning of the trunk or a combination of both.[4] The first compensatory mechanism is the increase in intersegmental LL by including more lumbar vertebrae in the lordotic segment, and when the maximal attainable LL is reached, the patient attempts to maintain a balanced posture by progressive retroversion of the pelvis.[4]

Having considered the role of abnormal spinopelvic arrangement, preliminary to any sagittal compensation is first the presence of an abnormal PI or SS.[4] PI is a morphological parameter and SS will only change degenerately. Neither parameter can, therefore, be considered as a compensatory mechanism. Conversely, PI and SS may be regarded as parameters indicative of an unstable biomechanical environment. The association of abnormal PI and SS with spondylolysis and low-grade spondylolisthesis may implicate them as prognostic factors in the progression from a lytic defect to vertebral slippage. However, evidence is yet to be presented that quantifies how abnormal PI or SS may create kinematic and deformational changes in the lumbar spine.

Here we use computed tomography (CT) data from a healthy human subject and nonlinear finite element (FE) modelling to create a 3-dimensional model of the lumbosacral spine, in an attempt to study the role of sacral slope in the progression of bilateral lytic defect at the L5 vertebra to spondylolisthesis from a biomechanical standpoint. We controlled for disc degeneration and PT variables that are also believed to be involved in the progression.[10-12] Since PT was controlled, any change in SS resulted in an equal change in PI. We hypothesized that variation in L5-S1 disc shape secondary to any variation in SS (while preserving the L5-S1 mid-disc height and the orientation of L5 vertebra) will create regional biomechanical instabilities conducive for the progression of bilateral lytic defect at the L5 vertebra to spondylolisthesis.

Materials and Methods

Image Segmentation and 3D Model Generation From CT Data

Prior approval from University of New South Wales Human Research Ethics Advisory Panel was obtained for the use of retrospectively acquired CT data from a human subject (NRR-HC16754). High-resolution lumbosacral spine CT data (437 axial cuts, 512 × 512 pixel resolution, slice thickness 0.50 mm) from an anonymized healthy male subject (26 years old) were obtained in DICOM (Digital Imaging and Communications in Medicine) file format from Carl Bryant Radiology, St. George Private Hospital, Sydney. The CT data was imported into image processing software Avizo Standard (version 8.1; FEI Visualization Sciences Group, Hillsboro, OR) for the segmentation of anatomical regions of interest, and subsequent generation and refinement of surface and volumetric meshes. Endplates were modelled with a sagittal plane depth of 1.00 mm (2 pixels), and the radial thickness of the 3 regions (outer, middle, inner) was assumed to be the same. The geometry of the intervertebral disc was approximated to include the region between the endplates. The nucleus pulposus was assumed to occupy approximately 43% of the disc volume and located slightly posterior to the center of the disc.[16]

The segmented CT data was manipulated to generate a bilateral L5 spondylolytic defect model by deleting pixels from the L5 pars region (LYTIC) creating an approximately 2-mm wide fracture gap between the bony fragments. Additionally, using the same protocols for creating L5 lytic defect, 2 more models were built to represent high and low sacral slopes. The image processing software did not allow for the rotation of the sacrum to alter SS; therefore, bone pixels on the sacrum were deleted from the anterior side and added to the posterior to increase SS by 10° (SS+10) and, conversely, to decrease SS by 10° (SS-10). By preservation of the sacral midpoint, PT was fixed, and therefore, any change in SS resulted in an equal change in PI. The objective was to model 3 different anatomical configurations (by modelling 3 distinct pelvic incidences) and not postural changes in the lumbar spine of one individual.

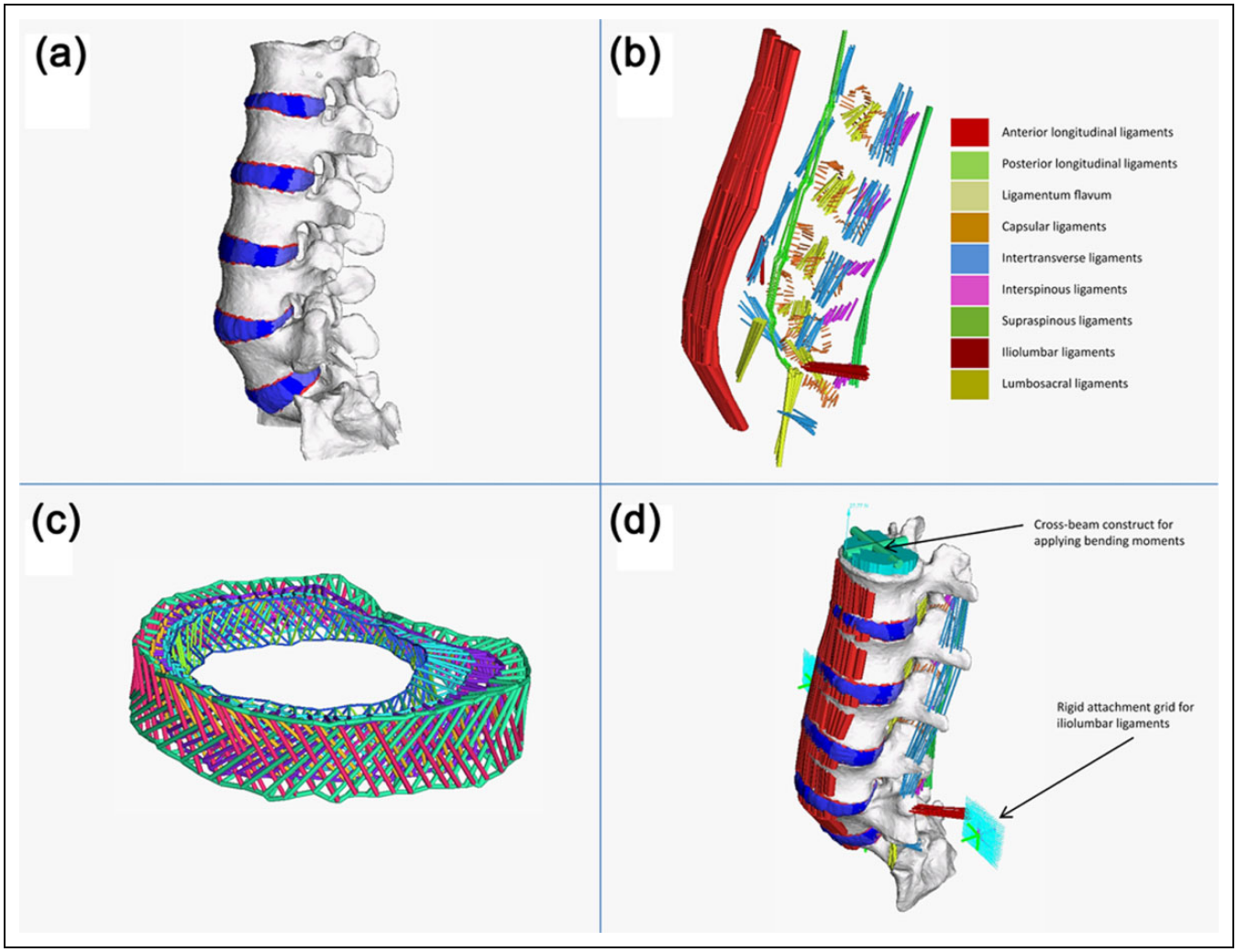

Figure 1. (a) A solid model of the lumbosacral spine comprising only the bony elements and the intervertebral discs. (b) Ligaments were modelled using nonlinear beam elements. (c) The concentric layers (n = 4) of crisscross collagen fibers modelled in the annulus fibrosus. (d) A fully preprocessed finite element model of the lumbosacral spine.

Modelling Annulus Fibers and Ligaments

Volumetric meshes in Nastran file format (.nas) representing different variants of the lumbosacral spine model were imported into the FE modelling software Strand7 (version 2.4.6, Strand7 Pty Ltd, Sydney, Australia; Figure 1a). The annulus fibrosus was modelled as a biphasic composite comprising concentric layers (n = 4) of crisscross collagen beam fibers embedded within a homogenous ground substance, with the ends of the fibers rigidly anchored in the superior and inferior endplates (Figure 1c). The collagen fiber volume fraction was assumed to linearly increase from 5% (of the annulus GS volume) in the innermost layer to 23% in the outermost layer.[17] The fiber diameters, which were averaged in each annulus layer, were based on the fiber volume fraction assumed, the number of beam elements used, and the volume of each annulus layer. Within each lamella, fiber angulations were varied from $\pm 24^{\circ}$ ventrally to $\pm 46^{\circ}$ dorsally representing histological findings.[18]

Ligaments were modelled using cylindrical beam elements, with the attachment and insertion sites based on previously recorded anatomical observations.[19] In order to minimize artefactual stress concentration at the attachment and insertion sites, ligaments were attached to the bone using a network of tessellated beams on the bone surface. In addition to the primary ligaments, iliolumbar (ILL) and lumbosacral ligaments (LSL) were also modelled. Since the geometry of the ilium was not created in the FE model, an artificial attachment site for the ILL fibers was created using a network of rigid links that was constrained in all rotational and translational degrees of freedom (Figure 1b). The type and number of elements used in assembling various FE models are presented in Table 1.

Facet Joint Articulations and Pars Interarticularis Fracture Gap

The compressive load bearing characteristics of the bony articulating pillars at each facet joint were modelled using nonlinear

Table 1. Number of Elements Used in the 4 Finite Element Models of Lumbosacral Spine. The Concentric Rings of Annulus Fibers Were Modelled Using Nonlinear Beam Elements.

	Intact	L5 Lytic	SS+10	SS-10
Nodes	308 539	320 256	319 536	265 207
Brick element (4-noded tetrahedrons)	1 454 554	1 522 196	1 519 003	1 196 053
Facet articulation (nonlinear point contact elements)	5 per joint	5 per joint	5 per joint	5 per joint
Bilateral L5 lytic defect (nonlinear contact zero gap elements)	0	20 per side	20 per side	20 per side
Annulus fibers (cylindrical beam elements)				
L1-L2	(O) 312-321-293-266 (I)	(O) 289-272-229-224 (I)	(O) 242-214-195-177 (I)	(O) 254-202-211-172 (I)
L2-L3	(O) 362-385-347-287 (I)	(O) 271-266-254-168 (I)	(O) 217-206-209-168 (I)	(O) 226-208-219-186 (I)
L3-L4	(O) 330-298-232-240 (I)	(O) 265-244-212-189 (I)	(O) 225-216-247-153 (I)	(O) 238-237-218-184 (I)
L4-L5	(O) 308-331-303-237 (I)	(O) 251-218-233-163 (I)	(O) 244-230-206-167 (I)	(O) 256-226-203-186 (I)
L5-S1	(O) 243-258-236-219 (I)	(O) 202-192-169-167 (I)	(O) 187-220-187-173 (I)	(O) 178-210-171-168 (I)
Ligaments per level (cylindrical beam elements)				
ALL	14	14	14	14
PLL	6	6	6	6
TL	16	16	16	16
LF	18	18	18	18
ISL	9	9	9	9
SSL	4	4	4	4
CL	24 per joint	24 per joint	24 per joint	24 per joint
ILL	20	20	20	20
LSL	22	22	22	22

Abbreviations: (O) Layer 1 (outermost)-Layer 2-Layer 3-Layer 4 (innermost) (I); ALL, anterior longitudinal ligament; PLL, posterior longitudinal ligament; TL, transverse ligament; LF, ligamentum flavum; ISL, interspinous ligament; SSL, supraspinous ligament; CL, capsular ligament; ILL, iliolumbar ligament; LSL, lumbosacral ligament.

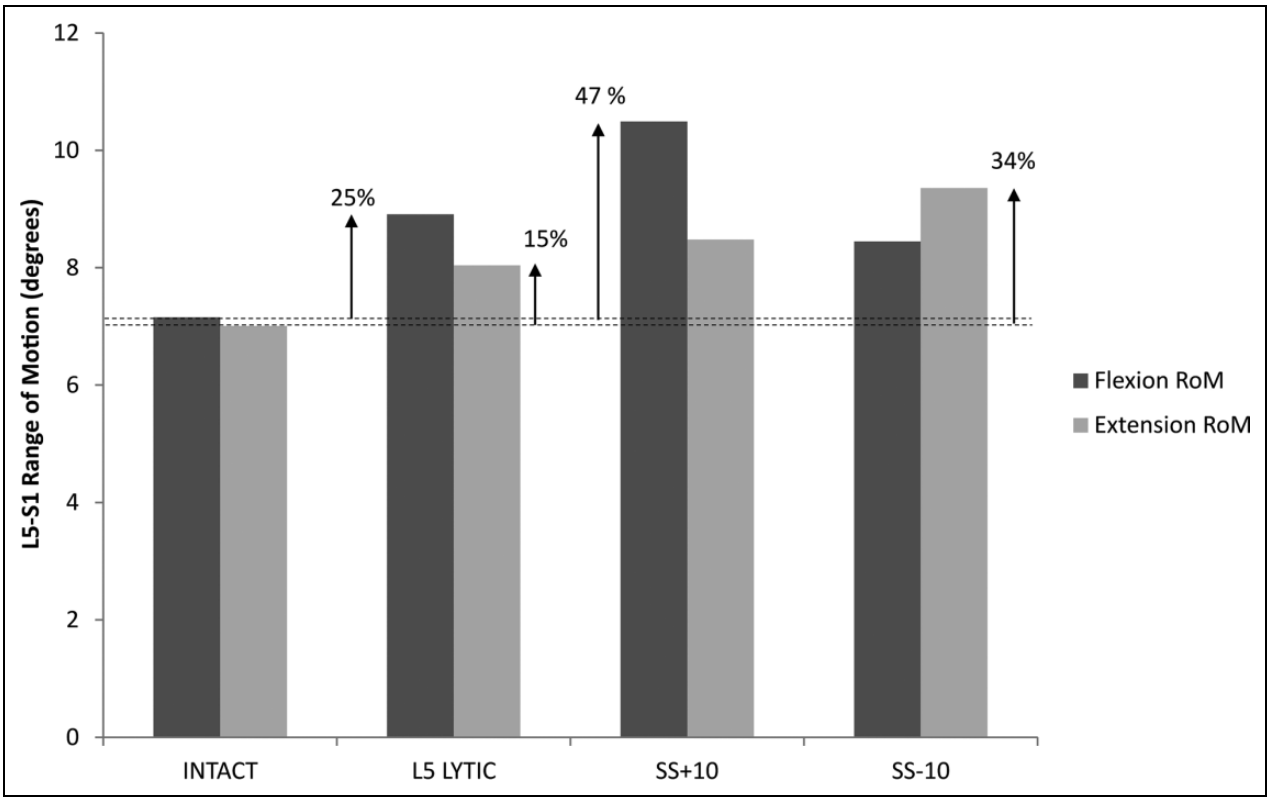

Figure 2. L5-S1 range of motion (RoM) in flexion (Fx) and extension (Ex) bending modes at peak loading (10 N m). The presence of a bilateral spondylolytic defect in the L5 vertebra increased RoM in both Fx and Ex. Compared with the normal LYTIC model, RoM increased in the SS+10 model during Fx, and in the SS-10 model during Ex.

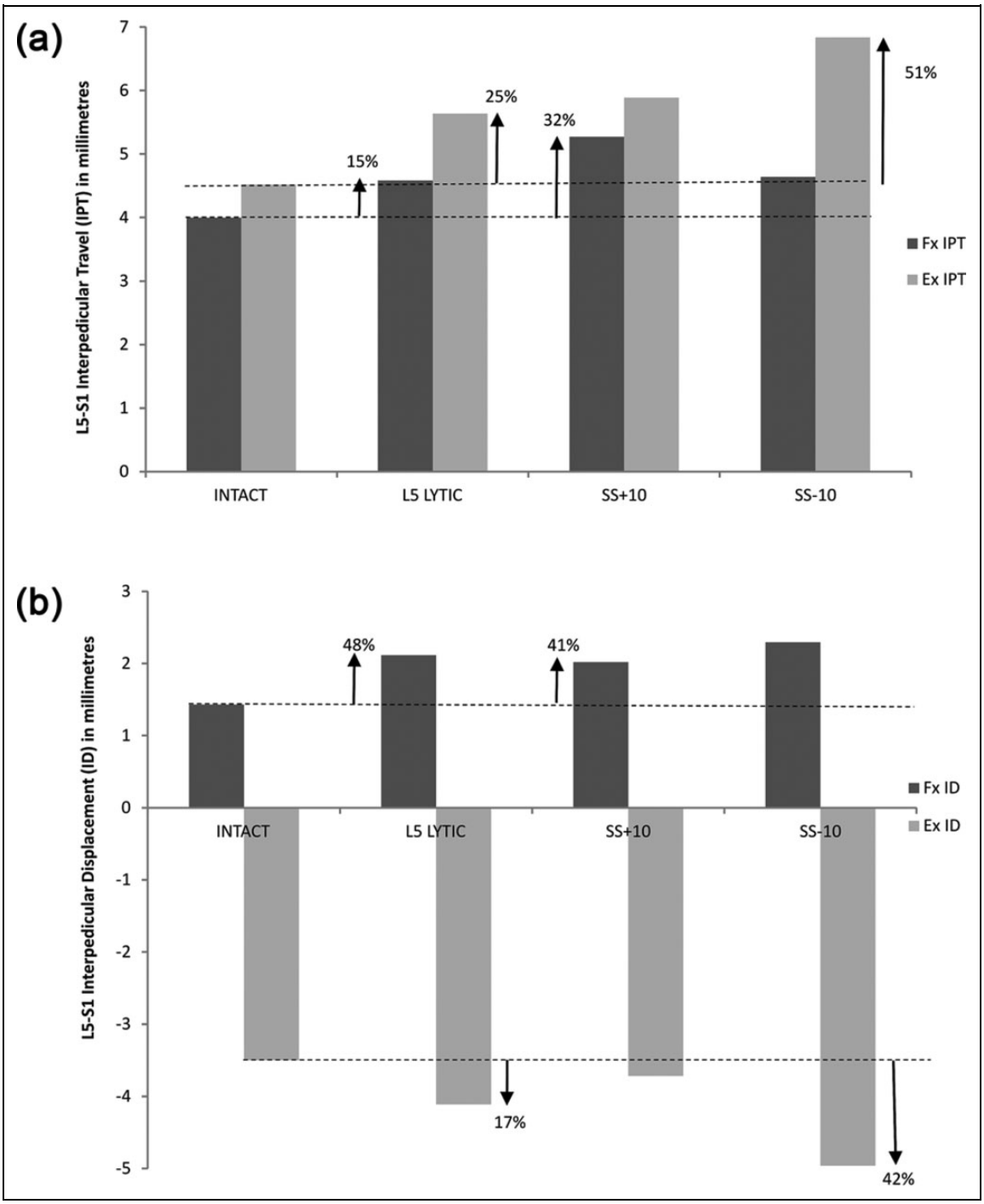

Figure 3. (a) L5-S1 interpedicular travel (IPT) in flexion (Fx) and extension (Ex) bending modes at peak loading (10 N m). The IPT metric captures the translational movement of a vertebra by measuring the movement of a pedicle with respect to the caudal pedicle. The bilateral L5 lytic defect increased IPT in both Fx and Ex. Compared with the normal LYTIC model, IPT increased in the SS+10 model during Fx, and in the SS-10 model during Ex. (b) L5-S1 ID in Fx and Ex bending modes at peak loading (10 N m). The ID metric captures translational deflection between adjacent segment pedicles in going from neutral to extreme position. The bilateral L5 spondylolytic defect increased ID in both Fx and Ex bending modes. Compared with the normal LYTIC model, the SS-10 model experienced a significant increase in ID during Ex.

contact elements in Strand7 (n = 5 per joint), which were normally oriented and uniformly distributed over the articulating surfaces. The bilateral pars interarticularis fracture gap in the LYTIC, SS+10, and SS-10 models was connected using nonlinear contact elements (n = 25 each side, compressive stiffness only) to allow for load transfer between the fractured fragments in the event of gap closure during simulated bending motions.

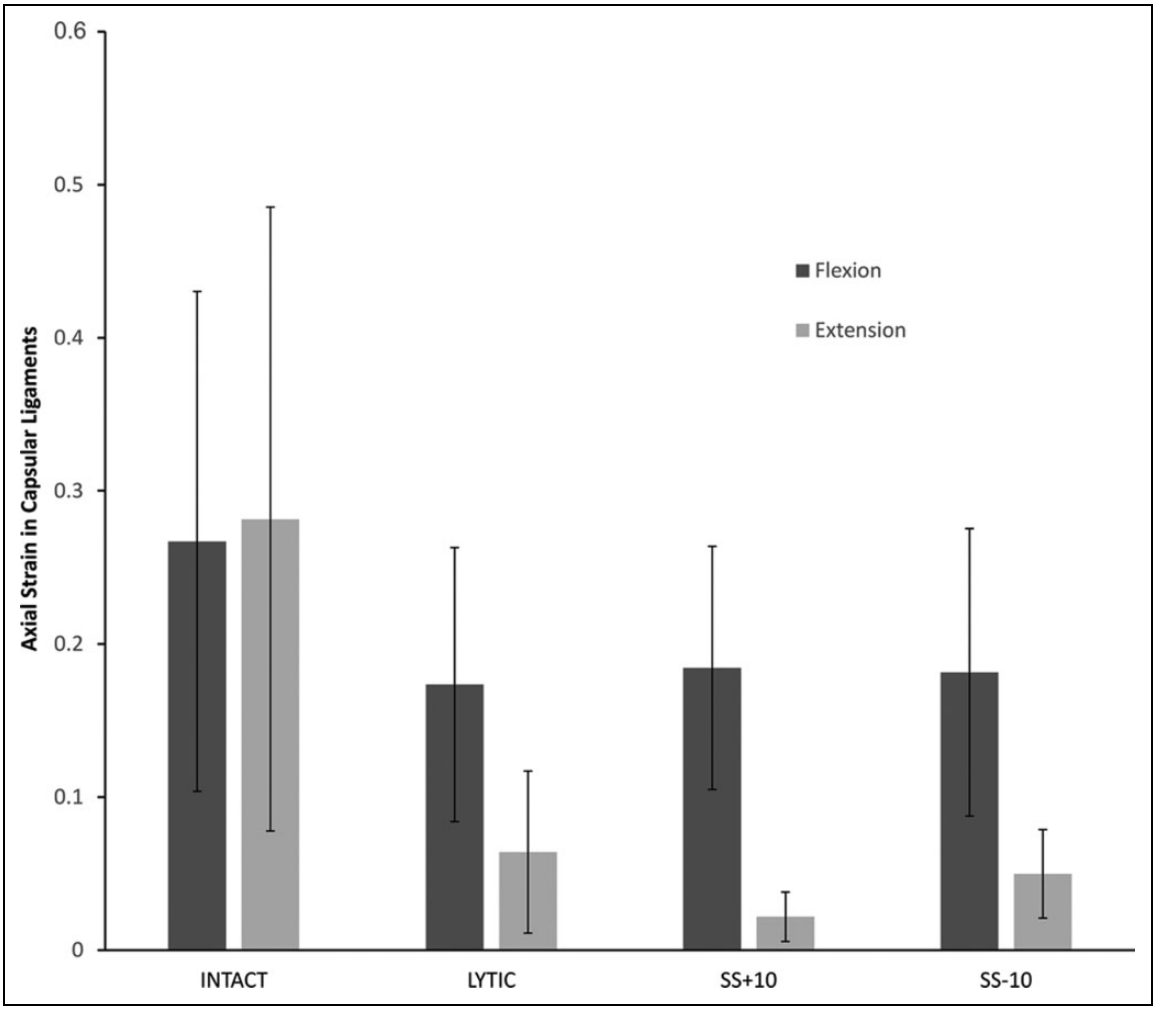

Figure 4. Axial strain in capsular ligaments under peak loading (10 N m) in flexion (Fx) and extension (Ex). The presence of a bilateral L5 spondylolytic defect significantly decreased capsular ligament strain in Fx and to a larger extent in Ex. Compared with the normal LYTIC model, changes in SS did not produce any significant change in capsular ligament strain. Error bars represent standard deviation.

Loads and Boundary Constraints

In all the models, a center node on the anterior surface of the sacral mass was fixed in all translational and rotational degrees of freedom. Bending motions were simulated using a cross-beam construct accommodated on the L1 superior endplate by means of a surface cap, both of which were assigned stainless steel material properties ($E = 200$ GPa, $\nu = 0.25$). A force couple was applied using the extreme nodes of the cross-beam to simulate flexion (Fx) and extension (Ex) bending motions (Figure 1d). The models were loaded in pure unconstrained moments (without any compressive preload) with stepwise increments in load from 1.0 N m to 10 N m.

The preprocessed FE models were solved for geometry, material, and boundary nonlinearities using the nonlinear static solver in Strand7.

Calibration of Material Property Values

A pilot study was conducted to calibrate material property values assigned to brick elements representing the intervertebral disc, beam elements representing the primary ligaments, and nonlinear contact elements representing facet articulation between the bony pillars (see Supplemental Material, available in the online version of the article). Using modelling protocols described above, an L3-L4 functional spinal unit (FSU) was assembled to simulate different stages of stepwise reduction of anatomical structures as presented previously.[20] The FE models were solved using the loads and boundary conditions described in the in vitro study, and numerical range of motion (RoM) results were compared with the in vitro results.[20] A closed loop optimization algorithm (illustrated in Supplemental Material, available in the online version of the article) was formulated to calibrate the material property values for the anatomical structure added at each stage of stepwise addition, in order to achieve a numerical RoM that was comparable with the in vitro RoM.

Results

The results were analyzed at peak Fx and Ex load (10 N m) in all the 4 models.

Table 2. Mean Axial Strain in the Posterior Ligaments During Peak Flexion Loading (10 N m)[a].

	Flexion					
	LF (±SD)	PLL (±SD)	ISL (±SD)	SSL (±SD)	LSL (±SD)	ILL (±SD)
Intact	0.11 (±0.01)	0.06 (±0.01)	0.32 (±0.03)	0.19 (±0.01)	0.00 (±0.00)	0.06 (±0.02)
Lytic	0.14 (±0.02)	0.10 (±0.01)	0.21 (±0.04)	0.12 (±0.00)	0.00 (±0.00)	0.08 (±0.02)
SS+10	0.13 (±0.01)	0.10 (±0.02)	0.25 (±0.03)	0.12 (±0.00)	0.00 (±0.00)	0.08 (±0.02)
SS-10	0.15 (±0.03)	0.09 (±0.00)	0.21 (±0.04)	0.10 (±0.01)	0.00 (±0.00)	0.07 (±0.02)

Abbreviations: SD, standard deviation; LF, ligamentum flavum; PLL, posterior longitudinal ligament; ISL, interspinous ligament; SSL, supraspinous ligament; LSL, lumbosacral ligament; ILL, iliolumbar ligament.
[a]The presence of bilateral spondylolytic defect at L5 significantly increased axial strain in the PLL and the LF.

L5-S1 Range of Motion

Comparing the INTACT model with the normal LYTIC, the L5-S1 RoM increased from 7.2° to 8.9° and from 7.0° to 8.0° in Fx and Ex bending modes, respectively. The Fx RoM in the SS+10 model was 10.5°, and the Ex RoM in the SS-10 model was 9.4°. The L5-S1 RoM results for all the 4 models are presented in Figure 2.

L5-S1 Interpedicular Kinematics

The L5-S1 interpedicular kinematic parameters in Fx and Ex were evaluated per published protocols.[21,22] Comparing the INTACT model with the normal LYTIC, the bending-plane interpedicular travel (IPT) parameter, measured in millimeters,[23] increased from 4.0 mm to 4.6 mm and from 4.5 mm to 5.6 mm in Fx and Ex bending modes, respectively. The Fx IPT in the SS+10 model was 5.3 mm, and the Ex IPT in the SS-10 model was 6.8 mm. The IPT results for all the 4 models are presented in Figure 3a.

Comparing the INTACT model with the normal LYTIC, the interpedicular displacement (ID) parameter increased from 1.4 mm to 2.1 mm and decreased from −3.5 mm to −4.1 mm in Fx and Ex bending modes, respectively. The Fx ID in the SS+10 model was 2.0 mm, and the Ex ID in the SS-10 model was −5.0 mm. The ID results for all the 4 models are presented in Figure 3b.

Axial Strain in Capsular Ligaments at the L5-S1 Level

Comparing the INTACT model with the normal LYTIC, mean axial strain in the capsular ligaments (CL) decreased from 0.27 (±0.16) to 0.17 (±0.09) and 0.28 (±0.20) to 0.06 (±0.05) in Fx and Ex bending modes, respectively. Compared with the normal LYTIC model, alterations in SS demonstrated insignificant changes in axial strain during Fx (SS+10: 0.18 [±0.08], SS-10: 0.18 [±0.09]). Axial strain in CL during Ex decreased to 0.02 (±0.02) in the SS+10 model and to 0.05 (±0.03) in the SS-10 model. Axial strain (CL) values at the L5-S1 level for all the 4 models are presented in Figure 4.

Axial Strain in Posterior Ligaments at the L5-S1 Level

Axial strain in the posterior ligaments at the L5-S1 level is presented in Tables 2 and 3. Comparing the INTACT model with the normal LYTIC, mean axial strain in ligamentum flavum (LF) fibers increased from 0.11 (±0.01) to 0.14 (±0.02) during Fx. Changes in LF axial strain due to alterations in SS, however, were insignificant when compared with the normal LYTIC model. The posterior longitudinal ligament (PLL) also demonstrated an increase (INTACT to normal LYTIC) in mean axial strain from 0.06 (±0.01) to 0.10 (±0.01) during Fx, but alterations in SS produced insignificant changes in PLL axial strain when compared with the normal LYTIC model. No significant changes in mean axial strain were observed in the posterior or anterior ligaments during Ex.

Table 3. Mean Axial Strain in the LSL, ILL, and ALL During Peak Extension Loading (10 N m).

	Extension		
	LSL (±SD)	ILL (±SD)	ALL (±SD)
Intact	0.00 (±0.00)	0.00 (±0.00)	0.05 (±0.01)
Lytic	0.00 (±0.00)	0.00 (±0.00)	0.06 (±0.01)
SS+10	0.00 (±0.00)	0.02 (±0.01)	0.05 (±0.01)
SS-10	0.00 (±0.00)	0.02 (±0.00)	0.06 (±0.01)

Abbreviations: SD, standard deviation; LSL, lumbosacral ligament; ILL, iliolumbar ligament; ALL, anterior longitudinal ligament.

Normal Stresses at the L5-S1 Level

Compressive and tensile stresses were evaluated separately for the L5-S1 disc. The color coded distribution of normal stresses on the L5-S1 mid-discal plane is shown in Figure 5. In all the 4 models, approximately two thirds of the mid-discal plane area was loaded in compression during Fx and Ex (range Fx: 64% to 71%; range Ex: 59% to 70%). Compared with the INTACT model, average compressive stress increased in the normal LYTIC model in Fx (0.11 MPa to 0.13 MPa) and Ex (0.15 MPa to 0.21 MPa). During Ex, the greatest compressive stress was observed in the SS+10 model (average: 0.30 MPa) with an abnormal stress concentration in the posterior annulus. During Fx, the greatest compressive stress was observed in the SS-10 model (average: 0.17 MPa) with an abnormal stress concentration in the anterior annulus.

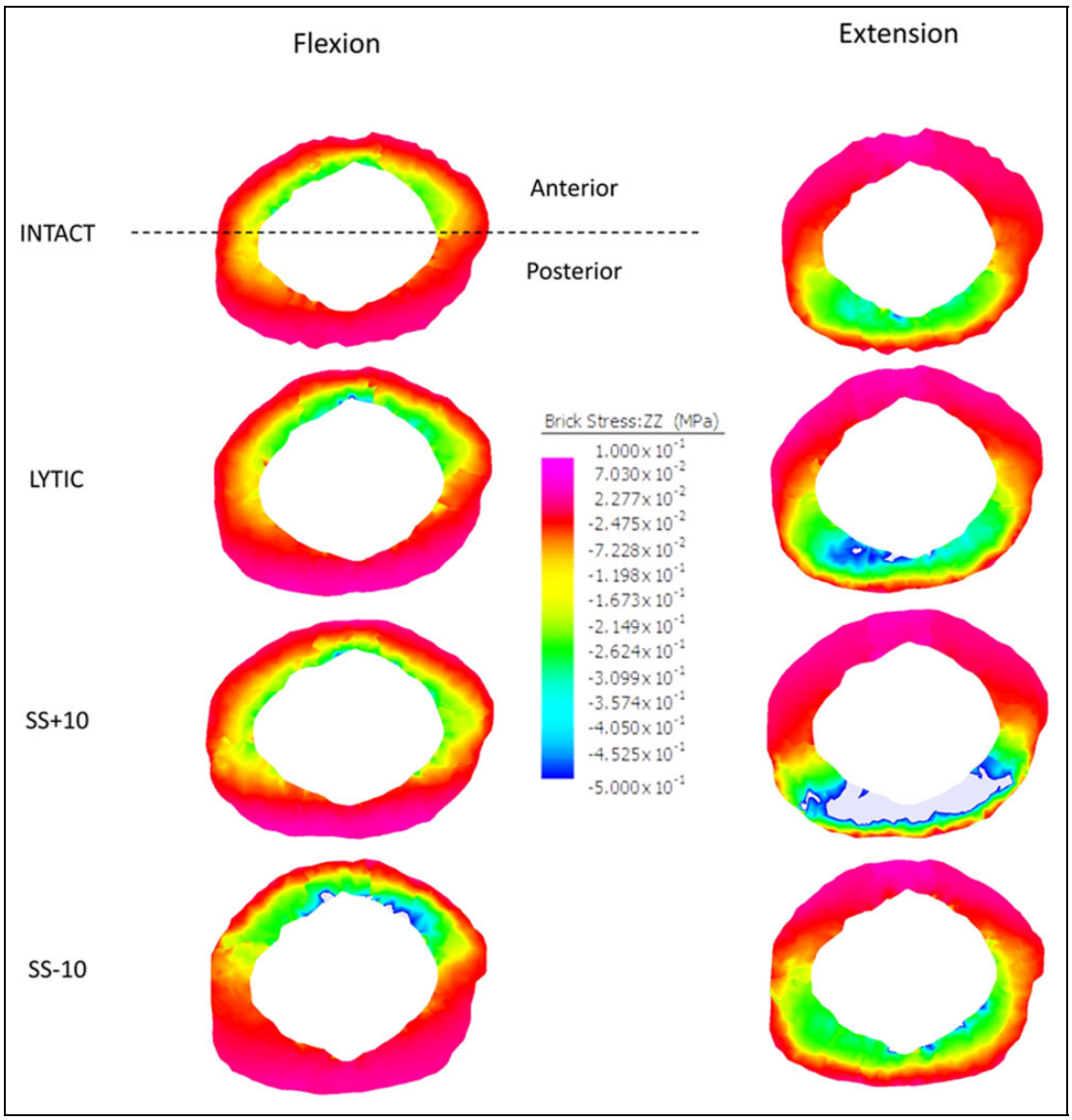

Figure 5. Normal stresses in the mid-discal plane of the L5-S1 disc in flexion (Fx) and extension (Ex) bending modes at peak loading (10 N m). Compared with the normal LYTIC model, the anterior annulus was abnormally loaded in compression during Fx in the SS-10 model, and the posterior annulus was abnormally loaded in compression during Ex in the SS+10 model.

Mid-Discal Shear Stresses at the L5-S1 Level

Anteriorly and posteriorly directed shear stresses in the mid-discal plane of the L5-S1 disc were evaluated separately, with positive shear assumed to be in the posteroanterior direction. The color coded distribution of shear stresses on the L5-S1 mid-discal plane is shown in Figure 6. Comparing the normal LYTIC model with the INTACT, posteriorly directed shear force increased by 45% and anteriorly directed shear force decreased by 11% in Fx loading. In Ex loading, posteriorly directed shear force increased by 91% and anteriorly directed shear force increased by 26% compared with the INTACT model.

Discussion

The main objective of this study was to further elucidate the role of sacral slope in the progression of a bilateral spondylolytic defect at the L5 vertebra to spondylolisthesis from a biomechanical standpoint.

In agreement with previous findings, the results showed that the presence of a bilateral lytic defect in the lumbar spine significantly increases segmental motion, normal and shear stresses during Fx and Ex bending.[21,24,25] The loss in posterior tension band following the defect also resulted in an increase in anteriorly directed shear forces in the L5-S1 mid-discal plane during Fx (45% ↑) and Ex (91% ↑). However, directional biomechanical instabilities were induced at the L5-S1 level as a result of varying sacral slope. Wedging of the L5-S1 disc (SS+10) resulted in a significantly greater Fx motion compared with the normal LYTIC model (Fx RoM: 18% ↑; Fx IPT: 15% ↑), but Ex motion characteristics were similar. For similar Ex motion characteristics between normal LYTIC and SS+10

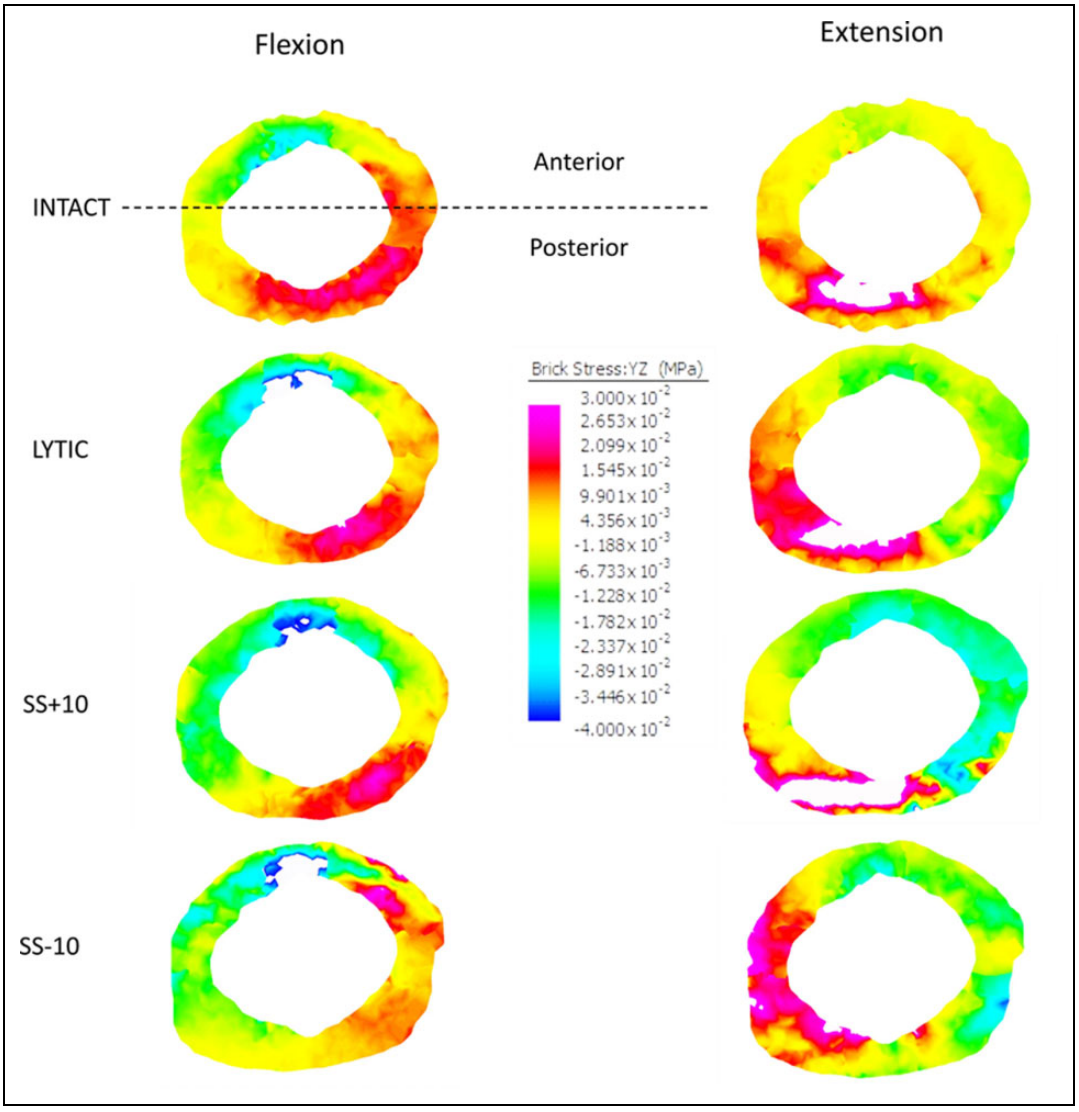

Figure 6. Posteroanterior (PA) directed shear stresses in the mid-discal plane of the L5-S1 disc in flexion (Fx) and extension (Ex) bending modes at peak loading (10 N m). Compared with the INTACT model, the loss in posterior tension band in the normal LYTIC model resulted in a decrease in area under positive PA shear stress in Fx (69% to 51%) and Ex (78% to 48%).

models, the average compressive stress in the L5-S1 disc was significantly higher (39% ↑) in the SS+10 model, with an abnormal stress concentration in the posterior annulus region likely due to reduced posterior disc height (Figures 2 and 5). Conversely, flattening of the L5-S1 disc (SS-10) resulted in a significantly greater Ex motion compared with the normal LYTIC model (Ex RoM: 16% ↑; Ex IPT: 21% ↑), but Fx motion characteristics were similar. For similar Fx motion characteristics between normal LYTIC and SS-10 models, the average compressive stress in the L5-S1 disc was significantly higher (24% ↑) in the SS-10 model, with an abnormal stress concentration in the anterior annulus region likely due to reduced anterior disc height (Figures 2 and 5).

Variation in SS while preserving the L5-S1 mid-disc height and orientation of the L5 vertebra will result in a change in the L5-S1 disc shape (Figure 7). Secondary to an increase in SS is an increase in wedging of the L5-S1 disc, which may cause a further impingement on the posterior annulus in addition to that achieved by lumbar lordosis. Conversely, a decrease in SS resulted in a flattening of the L5-S1 disc, which may produce an effect opposite to that of wedging and counteract natural lumbar lordosis. With a bilateral lytic defect at L5, increased wedging of the L5-S1 disc resulted in greater flexion movement and higher compressive stresses (in the posterior annulus region) during extension, whereas increased flattening of the L5-S1 disc resulted in greater extension movement and higher compressive stresses (in the anterior annulus region) during flexion. We posit that variation in sacral slope from normal (resulting in a change in the L5-S1 disc shape) creates directional biomechanical instabilities in the lumbosacral spine that are implicated in the progression of a bilateral lytic defect at the L5 vertebra to spondylolisthesis. With increased wedging of

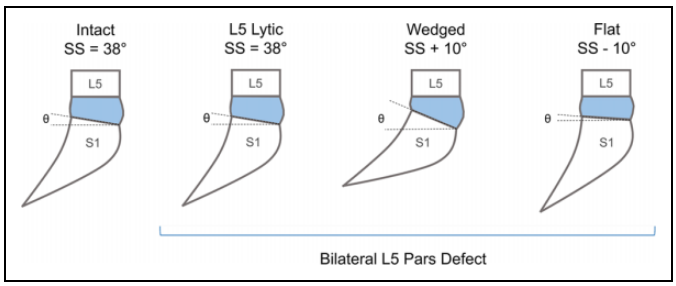

Figure 7. Changes in the L5-S1 disc shape secondary to the changes in sacral slope (SS). In all the models, the mid-disc height and the orientation of the L5 vertebra were kept the same.

the L5-S1 disc (SS+10), excessive compressive stresses in the posterior annulus during Ex may cause localized microtrauma to the disc tissues, which over repetitive loading could accumulate into tissue injury or loss in mechanical integrity.[26,27] This combined with a greater Fx movement may compromise the disc's ability to resist shear forces and hence result in the progression of the defect to spondylolisthesis. Conversely, with increased flattening of the L5-S1 disc (SS-10), tissue overloading and trauma may occur in the anterior annulus during Fx, which combined with greater Ex movement may compromise the disc's ability to resist shear forces and hence result in the progression of the defect to spondylolisthesis. The results suggest that for these extremities in the L5-S1 disc shape, different pathomechanisms exist that lead to the progression of the defect to spondylolisthesis.

Representative values for high and low sacral slopes have been reported by Labelle et al within the Spinal Deformity Study Group (SDSG).[4] The SDSG database represents a multicenter cohort of L5-S1 spondylolisthesis patients with different grades of listhesis, and the average values reported by the group for low and high sacral slopes are 35 $\pm$ 4° and 45 $\pm$ 4°, respectively.[4] In the averages reported by the SDSG, 28° represented a low sacral slope (SS-10), and 48° represented a high sacral slope (SS+10), both modified from the 38° SS of the INTACT state in the present study. Due to the changes in SS and the fixed orientation of the L5 vertebra, lumbar lordosis was not fixed. By altering the SS, lumbar lordosis also changed in different FE models (lumbar lordosis in the normal SS, high SS [wedged], and low SS [flat] models were 38.0°, 47.8°, and 26.9°, respectively).

Radiographic studies have shown that abnormality in spinopelvic morphology and orientation is implicated in the development of a lytic defect in the L5 vertebra and its progression to spondylolisthesis.[3,4,6] Such studies have primarily considered the orientation of the sacrum in respect of pelvis, and subsequent effects on the shear stresses in the L5-S1 disc. However, to the best of our knowledge, the importance of the L5-S1 disc shape in providing biomechanical stability to the lumbosacral region has not been studied previously.

The results from the present study are only valid for changes in the L5-S1 disc shape secondary to the changes in sacral slope. The shape of the L5-S1 disc may also change due to a change in the orientation of the L5 vertebra alone, or a combination of change in sacral slope and orientation of the L5 vertebra, and it remains to be seen whether these will also induce similar biomechanical changes in the lumbosacral spine during flexion and extension bending. The study was further limited by the absence of femoral heads in the obtained CT data, which prevented the measurement of PI and PT.

Conclusions

In conclusions, changes in the L5-S1 disc shape secondary to the changes in sacral slope resulted in different biomechanical environments in the lumbosacral spine, which may lead to different pathomechanisms for the progression of the L5 bilateral lytic defect to spondylolisthesis. Compared with a normal LYTIC defect model, increased wedging of the L5-S1 disc (SS+10) resulted in greater Fx movement and increased stresses in posterior annulus during Ex, whereas flattening of the L5-S1 disc (SS-10) resulted in greater Ex movement and increased stresses in anterior annulus during Fx. Further radiographic studies are required to confirm these findings, but if true, this suite of biomechanical changes in the lumbosacral spine will need to be considered in the prognosis of patients with this defect condition, and ultimately guide the course of clinical treatment.

Acknowledgments

The authors thank Emma Wheatley, Karen Ruut, and Carl Bryant from CJ Bryant Radiology, St. George Private Hospital, Sydney, Australia, for providing access to de-identified patient CT data.

Declaration of Conflicting Interests

The author(s) declared no potential conflicts of interest with respect to the research, authorship, and/or publication of this article.

Funding

The author(s) disclosed receipt of the following financial support for the research, authorship, and/or publication of this article: This work was supported by a research grant from AO Spine Foundation Asia Pacific (AOSAUNZ(R) 2016-01), a Taste of Summer Research Scholarship from UNSW Australia to VR, an International Postgraduate Research Scholarship from UNSW Australia and DIISRTE to UC, and internal research funds from Spine Service.

Supplemental Material

The supplemental material is available in the online version of the article.

References

1. Fredrickson BE, Baker D, McHolick WJ, Yuan HA, Lubicky JP. The natural history of spondylolysis and spondylolisthesis. *J Bone Joint Surg Am*. 1984;66:699-707.
2. Leone A, Cianfoni A, Cerase A, Magarelli N, Bonomo L. Lumbar spondylolysis: a review. *Skeletal Radiol*. 2011;40:683-700.
3. Roussouly P, Gollogly S, Berthonnaud E, Labelle H, Weidenbaum M. Sagittal alignment of the spine and pelvis in the presence

of L5-s1 isthmic lysis and low-grade spondylolisthesis. *Spine (Phila Pa 1976)*. 2006;31:2484-2490.
4. Labelle H, Mac-Thiong JM, Roussouly P. Spino-pelvic sagittal balance of spondylolisthesis: a review and classification. *Eur Spine J*. 2011;20(suppl 5):641-646.
5. Hresko MT, Labelle H, Roussouly P, Berthonnaud E. Classification of high-grade spondylolistheses based on pelvic version and spine balance: possible rationale for reduction. *Spine (Phila Pa 1976)*. 2007;32:2208-2213.
6. Mac-Thiong JM, Labelle H. A proposal for a surgical classification of pediatric lumbosacral spondylolisthesis based on current literature. *Eur Spine J*. 2006;15:1425-1435.
7. Vialle R, Ilharreborde B, Dauzac C, Lenoir T, Rillardon L, Guigui P. Is there a sagittal imbalance of the spine in isthmic spondylolisthesis? A correlation study. *Eur Spine J*. 2007;16:1641-1649.
8. Farfan HF, Osteria V, Lamy C. The mechanical etiology of spondylolysis and spondylolisthesis. *Clin Orthop Relat Res*. 1976; (117):40-55.
9. Ikata T, Miyake R, Katoh S, Morita T, Murase M. Pathogenesis of sports-related spondylolisthesis in adolescents. Radiographic and magnetic resonance imaging study. *Am J Sports Med*. 1996;24:94-98.
10. Szypryt EP, Twining P, Mulholland RC, Mulholland RC, Worthington BS. The prevalence of disc degeneration associated with neural arch defects of the lumbar spine assessed by magnetic resonance imaging. *Spine (Phila Pa 1976)*. 1989;14:977-981.
11. Floman Y. Progression of lumbosacral isthmic spondylolisthesis in adults. *Spine (Phila Pa 1976)*. 2000;25:342-347.
12. Seitsalo S, Schlenzka D, Poussa M, Osterman K. Disc degeneration in young patients with isthmic spondylolisthesis treated operatively or conservatively: a long-term follow-up. *Eur Spine J*. 1997;6:393-397.
13. Stone AT, Tribus CB. Acute progression of spondylolysis to isthmic spondylolisthesis in an adult. *Spine (Phila Pa 1976)*. 2002;27: E370-E372.
14. Lyras DN, Tilkeridis K, Stavrakis T. Progression of spondylolysis to isthmic spondylolisthesis in an adult without accompanying disc degeneration: a case report. *Acta Orthop Belg*. 2008;74:141-144.
15. Oh YM, Choi HY, Eun JP. The comparison of sagittal spinopelvic parameters between young adult patients with L5 spondylolysis and age-matched control group. *J Korean Neurosurg Soc*. 2013; 54:207-210. doi:10.3340/jkns.2013.54.3.207.
16. White AA, Panjabi MM. *Clinical Biomechanics of the Spine*. 2nd ed. New York, NY: JB Lippincott; 1990.
17. Lu YM, Hutton WC, Gharpuray VM. Do bending, twisting, and diurnal fluid changes in the disc affect the propensity to prolapse? A viscoelastic finite element model. *Spine (Phila Pa 1976)*. 1996; 21:2570-2579.
18. Cassidy JJ, Hiltner A, Baer E. Hierarchical structure of the intervertebral disc. *Connect Tissue Res*. 1989;23:75-88.
19. Behrsin JF, Briggs CA. Ligaments of the lumbar spine: a review. *Surg Radiol Anat*. 1988;10:211-219.
20. Heuer F, Schmidt H, Klezl Z, Claes L, Wilke HJ. Stepwise reduction of functional spinal structures increase range of motion and change lordosis angle. *J Biomech*. 2007;40:271-280.
21. Chamoli U, Chen AS, Diwan AD. Interpedicular kinematics in an in vitro biomechanical assessment of a bilateral lumbar spondylolytic defect. *Clin Biomech (Bristol, Avon)*. 2014;29:1108-1115.
22. Chamoli U, Chen AS, Diwan AD. Letter to the Editor regarding the article "Interpedicular Travel in the Evaluation of Spinal Implants: An application in Posterior Dynamic Stabilization" by D.J. Cook, M.S. Yeager, and B.C. Cheng: Spine 2012;37(11):923-931. *Spine (Phila Pa 1976)*. 2014;39:921.
23. Schmidt H, Heuer F, Drumm J, Klezl Z, Claes L, Wilke HJ. Application of a calibration method provides more realistic results for a finite element model of a lumbar spinal segment. *Clin Biomech (Bristol, Avon)*. 2007;22:377-384.
24. Wang JP, Zhong ZC, Cheng CK, et al. Finite element analysis of the spondylolysis in lumbar spine. *Biomed Mater Eng*. 2006;16: 301-308.
25. Mihara H, Onari K, Cheng BC, David SM, Zdeblick TA. The biomechanical effects of spondylolysis and its treatment. *Spine (Phila Pa 1976)*. 2003;28:235-238.
26. Stokes IAF, Iatridis JC. Mechanical conditions that accelerate intervertebral disc degeneration: overload versus immobilization. *Spine (Phila Pa 1976)*. 2004;29:2724-2732.
27. Setton LA, Chen J. Mechanobiology of the intervertebral disc and relevance to disc degeneration. *J Bone Joint Surg Am*. 2006; 88(suppl 2):52-57.